Microphysical Interpretation of Multi-Parameter Radar Measurements in Rain. Part I: Interpretation of Polarization Measurements and Estimation of Raindrop Shapes

A. R. JAMESON

Illinois State Water Survey, Champaign, IL 61820

(Manuscript received 8 November 1982, in final form 25 March 1983)

ABSTRACT

The backscattered electric field received by a radar is related to the transmitted field by a backscatter matrix. In the case of single raindrops the elements in this matrix are determined by raindrop size and shape. At long radar wavelengths, certain combinations of elements, however, only depend on raindrop shape. These combinations form the basis of current linear and circular polarization measurables.

An ensemble of raindrops will usually exhibit a variety of shapes because of the variation in raindrop size and because of oscillations induced by drop oscillations. This shape variation can be described by an axis ratio distribution. Since at long wavelengths in rain the radar polarization measurables are largely determined by shape, they are sensitive to this axis ratio distribution. In this study, the sensitivity of some linear and circular polarization measurables to the mean and variance of the raindrop axis ratio distribution is investigated. These measurables are then used to formulate estimators of radar-power-weighted mean axis ratio and variance. These estimators appear to be applicable to a wide variety of drop size distributions.

1. Introduction

In the past several years an important development in radar meteorology has been the evolution of techniques for precipitation classification and more quantitative precipitation measurements. The two problems have been addressed using circular polarization radar measurements (McCormick *et al.*, 1972; Barge, 1974; Hendry and McCormick, 1974; McCormick and Hendry, 1975; Hendry *et al.*, 1976; McCormick and Hendry, 1979) and linear polarization radar measurements (Seliga and Bringi, 1976; Hall *et al.*, 1980; Goddard *et al.*, 1982).

McCormick *et al.* (1972) clearly established that rain forms a medium of predominately horizontally oriented, distorted scatterers. Seliga and Bringi (1976) subsequently proposed that the distortion of the raindrops should introduce a detectable difference between nearly simultaneous measurements of the reflectivity factors at two orthogonal, linear polarizations (i.e., vertical and horizontal), and that this information could be used for more quantitative measurements of rain. Regardless of the type of polarization used to obtain measurements, it is reasonable to expect that certain properties of rain should affect, to differing degrees, both circularly and linearly polarized transmissions.

At a radar wavelength of 10 cm, the characteristics of radar polarization measurements in rain are determined by the shapes of raindrops and their orientation. In the absence of other drops and in still air (or laminar flow wind tunnels), raindrops assume shapes that are exclusively a function of their equivalent diameters (Pruppacher and Beard, 1970; Pruppacher and Pitter, 1971). Although small drops (less than about 0.1 cm in diameter) are essentially spherical, larger drops become increasingly oblate as the diameter increases. Photographs of individual, natural raindrops (e.g., Jones, 1959), on the other hand, show that for each raindrop size there can be an assortment of shapes distributed about a mean oblate shape. In turbulent flow wind tunnels (Blanchard, 1950; Brook and Latham, 1968; Nelson and Gokhale, 1972) and in the free atmosphere near the ground (e.g., Blanchard, 1962), drops have been observed to oscillate. Although direct observations of raindrop oscillations above the surface layer have not been made, calculations suggest that, at times, collisions among drops are adequate to induce significant oscillations (Beard *et al.*, 1983). Such oscillations would tend to produce a distribution of shapes and not the single 'equilibrium' predicted by theory.

Wind tunnel studies (Blanchard, 1950; Brook and Latham, 1968; Nelson and Gokhale, 1972) and photographs of natural raindrops (e.g., Jones, 1959; Mueller and Sims, 1966) suggest that, often, drop shape can be approximated by oblate and prolate shapes. These shapes are characterized by an axis ratio r defined as the ratio of the magnitudes of the vertical to the horizontal axes. The assortment of shapes possible for any given drop mass can be expressed as an axis ratio distribution with a mean $\bar{r}$ and a variance σ_r^2. For oscillating raindrops, $\bar{r}$ will not necessarily be equivalent to their equilibrium shapes; $\bar{r}$ may deviate significantly from equilibrium (Jameson and Beard, 1982; Beard *et al.*, 1983).

The sensitivity of various radar polarization measurables to variations in $\bar{r}$ and σ_r^2 differ considerably. These differences suggest that several simultaneously measured polarization parameters might be used to estimate the radar power weighted analogues of both $\bar{r}$ and σ_r^2. Construction of appropriate estimators, however, requires some understanding of the characteristics of freely falling raindrops, the properties of axis ratio distributions, and the sensitivity of the particular polarization measurables to variations in the axis ratio distributions.

2. Axis ratio distributions

Little is known about the nature of the axis ratio distribution. Some information on raindrops of sizes 0.2 to 0.5 cm equivalent mass spherical diameter can be extracted from photographs of individual drops originally collected by Mueller and Sims (1966). These photographs provide direct measurements of drop shapes in the free atmosphere. They can be used to calculate the radar polarization characteristics of drop ensembles; they can also be used to investigate the sensitivity of a number of different radar polarization parameters to variations in $\bar{r}$ and σ_r^2.

a. Drop orientation

Although unusual transitory shapes can be expected to occur during raindrop oscillations, most observed shapes may be classified as either oblate or prolate. Since there is, as yet, little information concerning the frequency and exact shapes as the raindrops undergo complex motions, raindrop shapes will be characterized in all subsequent calculations as simple oblate or prolate spheroids.

In general, drops tend to fall with their axis of symmetry perpendicular to the ground. It is known, however, that raindrops may cant (axis of symmetry tilting away from the vertical) in regions of strong shear (Brussard, 1974; Maher *et al.*, 1977). Both theoretical consideration of the expected response of raindrops to atmospheric wind shear as well as microwave measurements, however, indicate that above the surface layer, raindrop canting angles are small (less than a few degrees) and narrowly distributed about a mean value near zero (Beard and Jameson, 1983). Although within a radar pulse volume some drops may be slightly canted, the average canting angle of the ensemble as a whole should stay near zero. The obvious exception, of course, is the 'artificial' canting introduced by the tilting of a radar antenna and, at long ranges, by the curvature of the earth. Since canting angle α usually appears in terms involving $\cos 2\alpha$ and $\sin 2\alpha$, radar elevation angles less than 5–10° will not introduce serious departures from the assumption of $\alpha = 0$. Since many observations of rain by meteorological radars will be at small elevation angles, the effect of antenna tilting will not be considered further.

b. Drop camera data

During the late 1950's and early 1960's, a camera system was used extensively to photograph raindrops. The resulting large data set consisted of drop-by-drop measurements of the maximum and minimum image dimensions. This information was subsequently used to estimate drop sizes and to determine drop size distributions (e.g., Mueller and Sims, 1966). More recently, Bresch (1982) reanalyzed the same data to estimate drop shapes. He found that the camera data provided useful and consistent information. Data from a number of locations were analyzed. The largest data set, collected in Miami, Florida, contained measurements of 128,826 drops of diameter greater than 0.2 cm diameter.

Fig. 1 (adapted from Bresch, 1982) is a plot of axis ratio distributions observed in Miami for three different drop size categories. The distribution of axis ratios (r) is a function of drop size. At the smaller size (0.23 cm) there is one clear frequency maximum. As the diameter increases, however, the distributions assume a bimodal or multimodal appearance. Although this change is certainly affected by the decreasing sample size, there is also an increasing separation between the mean and the "equilibrium" axis ratios. For example, in Fig. 1, the distribution corresponding to the drop diameter of 0.31 cm is particularly suggestive of one group of drops with equilibrium or near-equilibrium shapes and another group of drops with an average shape significantly offset from equilibrium. Different modes of raindrop oscillation may be responsible for much of the structure of distributions such as shown in Fig. 1. These oscillation modes, however, are not well understood. In this study, no attempt will be made to explain the details of the distributions. Instead, these observations will be used to investigate the sensitivity of various polarization parameters to $\bar{r}$ and σ_r^2. While use of measured distributions of r should add a touch of realism and realistic complexity to the calculations, the exact details of distributions are not likely to bias the results. An arbitrary set of drop axis ratios could have been used instead.

Fig. 2 shows the variation of $\bar{r}$ and σ_r^2 of the Miami drops as functions of equivalent volume diameter D. A least square errors fit to $\bar{r}$ is given by

$$\bar{r} = 1.01 - 0.23D, \quad 0.2 \leqslant D \leqslant 0.5 \text{ cm}, \quad (1a)$$

with a correlation coefficient of −0.96. For comparison, the equivalent expression for drops with equilibrium axis ratios r_E is given by (Pruppacher and Beard, 1970)

$$r_E = 1.03 - 0.62D, \quad D \geqslant 0.1 \text{ cm}. \quad (1b)$$

Fig. 2b shows the standard deviation of the axis ratio distribution, σ_r, as a function of the raindrop diameter. The main feature of that curve is the relative minimum at about 0.28 cm. Although this fea-

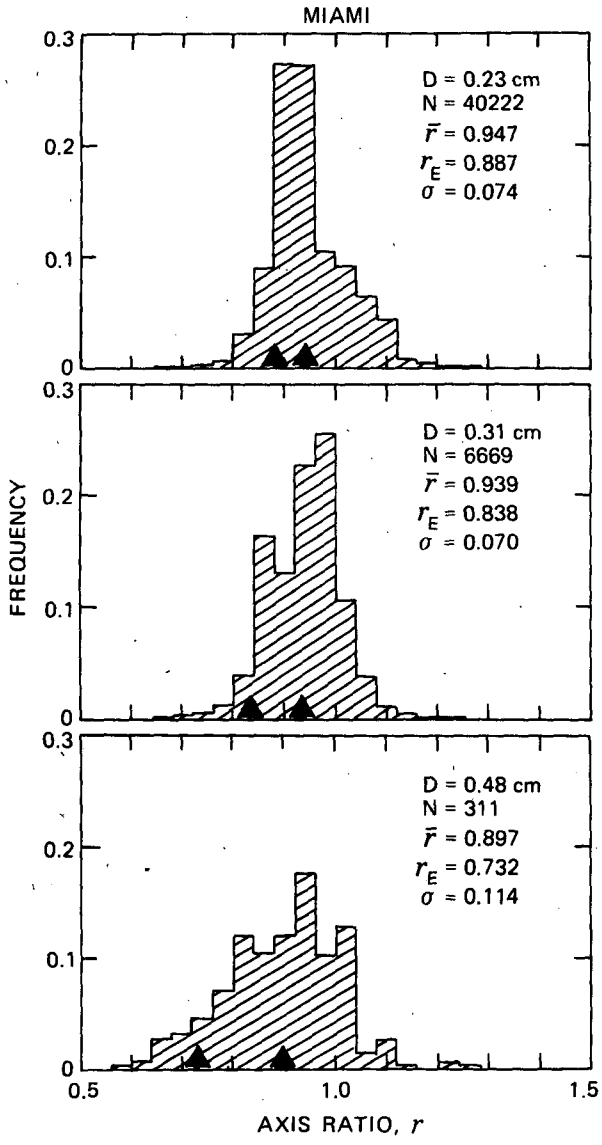

FIG. 1. Axis ratio histograms for three different drop diameters D. N is the number of drops included in each histogram, $\bar{r}$ and r_E are the average and equilibrium axis ratios. σ is the standard deviation of each histogram. The two symbols on the bottom locate r_E (left most one) and $\bar{r}$.

ture could be an artifact, it is not peculiar to this one set of data, and it may be a reflection of changes in the modes of oscillation with size (Beard, personal communication, 1982). The increase in σ_r beyond the minimum follows the enhanced separation between $\bar{r}$ and r_E with increasing diameter. Linear fits to the data yield

$$\sigma_r = 0.13 - 0.25D, \qquad 0.2 \leq D \leq 0.274 \text{ cm}, \quad (2a)$$

$$\sigma_r = -0.016 + 0.28D, \qquad 0.274 < D \leq 0.5 \text{ cm}, \quad (2b)$$

with correlation coefficients of −0.95 and 0.99, respectively.

3. Theoretically predicted polarization properties for monodisperse drop size distributions

The backscatter properties of a raindrop or collection of drops can be expressed in the form of a backscatter matrix of complex numbers (Deschamps, 1951)

$$\mathbf{S} = \begin{bmatrix} S_{22} & S_{21} \\ S_{12} & S_{11} \end{bmatrix}. \quad (3)$$

The backscatter electric field vector is the product of **S** and the incident electric field. A radar transmits an electric field which is polarized (usually linearly or circularly). In general, the backscattered electric field consists of two components, one polarized in the same sense as the transmission and the other polarized orthogonally (see Crispin and Siegel, 1968). Measurements of these two orthogonally polarized signals can be used to extract information about the shape of the scatterers. In the case of orthogonal linear signals, typically one electric field is polarized horizontally to the surface of the earth and the other vertically. In this case the diagonal elements S_{22} and S_{11} are responsible for almost all of the back-scattered return. The off-diagonal elements are associated with cross-polarized radar return signals (e.g., transmit vertically receive horizontally). In rain, these terms are very small.

It can be demonstrated (e.g., Crispin and Siegel, 1968) that the couplet of orthogonal circular polarizations (i.e., right-handed: left-handed) and the couplet of linear polarizations (horizontal: vertical) are transformations of one another. Thus, $\mathbf{S}_C$ and $\mathbf{S}_L$ (where C and L denote circular and linear polariza-

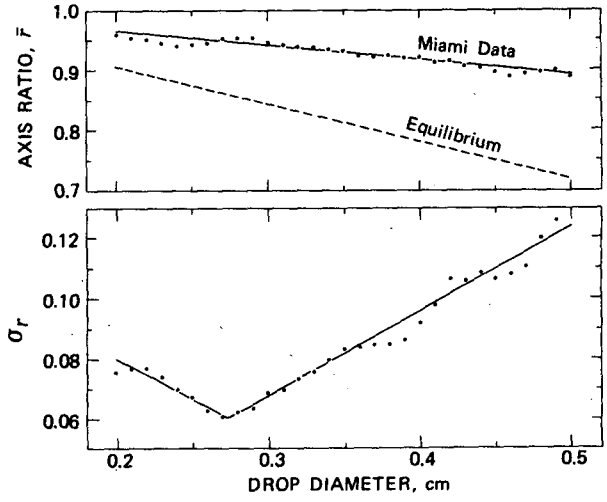

FIG. 2. (a) A plot of the average axis ratio $\bar{r}$ as a function of drop diameter for the Miami data. The dashed line corresponds to equilibrium drop shapes. The solid line is a least square error linear fit. (b) A plot of the standard deviation of the axis ratio distribution as a function of drop size for the Miami data. The solid lines are least square error linear fits.

tions, respectively) are also transformations of one another. This does not mean, however, that in the case of meteorological scatterers, polarization parameters measured by circularly and linearly polarized radars are equivalent. It will be seen, in fact, that each of the three most frequently used polarization parameters are sensitive to different moments of the axis ratio distribution. Therefore, even though the orthogonally polarized received signals may be transformed into one another, parameters derived from each of the polarizations contain different information.

a. Z_{DR}

One of the polarization variables of particular interest is differential reflectivity (Seliga and Bringi, 1976), derived from linear polarization measurements. For an ensemble of drops of equal size but of different r (as in Fig. 1, for example) the differential reflectivity for time averaged power returns is defined by

$$10^{(Z_{DR}/10)} = \frac{\int \sigma_H(r)dr}{\int \sigma_V(r)dr} = \frac{\int |S_{HH}|^2 f(r)dr}{\int |S_{VV}|^2 f(r)dr}, \quad (4)$$

where Z_{DR} is the differential reflectivity in dB, $f(r)dr$ is the fraction of drops with axis ratio between r and $r + dr$, $\sigma_H = 4\pi|S_{HH}|^2$ and $\sigma_V = 4\pi|S_{VV}|^2$ are the horizontal and vertical back-scatter cross-sections, respectively. The summation, in this case, is over all axis ratios.

Equation (4) was used to compute Z_{DR} for the axis ratio distributions observed in Miami. The complex forms of S_{HH} and S_{VV} were calculated using an updated version of the basic approach described in Warner and Hizal (1976). Three computations were performed. Here Z_{DR} was computed 1) using the full observed distribution of axis ratios, 2) using a Gaussian distribution with mean and standard deviation equal to the Miami values, and 3) only using the observed mean axis ratio $\bar{r}$. Fig. 3 shows that the results of all three methods of computing Z_{DR} are essentially equivalent. Z_{DR}, for all practical purposes, seems to be only a function of $\bar{r}$ and not σ_r.

The dependence on $\bar{r}$ alone is the result of considering raindrops which are small with respect to the radar wavelength. In that case, theory shows that the quantity $|S_{HH}|^2/|S_{VV}|^2$ is almost exclusively a function of $\bar{r}$. Using a program provided by Dr. Warner (personal communication, 1982) values of S_{HH} and S_{VV} were computed over a wide range of r at 10.71 cm wavelength. A power law fit between $|S_{HH}|^2/|S_{VV}|^2$ and r yields

$$\frac{|S_{HH}|^2}{|S_{VV}|^2} = r^{-7/3} \quad (5)$$

for $0.6 \leq r \leq 1.4$. This range of r encompasses almost

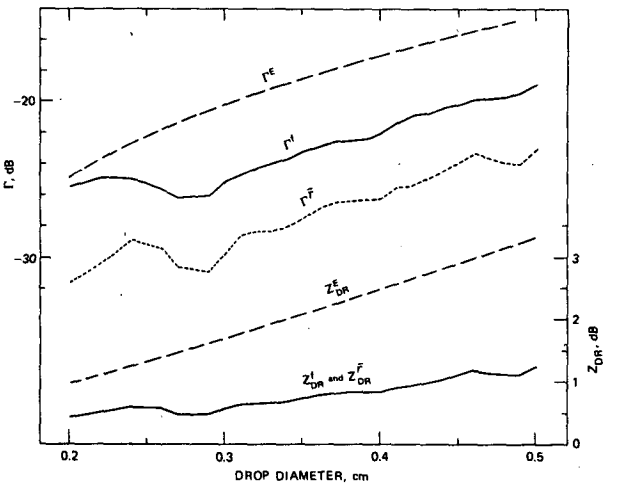

FIG. 3. Plots of Γ (CDR) and Z_{DR} as functions of drop diameter for the Miami data. Both quantities were calculated four ways. Two methods were based solely on a single axis ratio corresponding to each drop size. The corresponding curves are denoted by superscript E, for equilibrium axis ratio, and by superscript $\bar{r}$, for the mean axis ratio defined by (1a). Computations using the full distribution of axis ratios from the Miami data are indicated by superscript f. Computations using a Gaussian form of axis ratio distribution with a mean and variance prescribed by the Miami observations produced results essentially identical to those using the full, observed distribution. For Γ, computations based only on the average axis ratio differ substantially from those derived using the full axis ratio distribution.

all values actually observed for raindrops. Values of $|S_{HH}|^2/|S_{VV}|^2$ computed from (5) are compared to actual values in Table 1. Using (5), (4) becomes

$$10^{(-Z_{DR}/10)} = \frac{\int r^{7/3}|S_{HH}|^2 f(r)dr}{\int |S_{HH}|^2 f(r)dr} \quad (6a)$$

$$= \mathcal{R}^{7/3}, \quad (6b)$$

where $\mathcal{R}$ denotes a power $[|S_{HH}|^2]$ weighted average. Thus, for a monodisperse size distribution of drops and at long radar wavelengths, Z_{DR} is simply a function of the power weighted mean axis ratio $\mathcal{R}$.

TABLE 1. Comparison of radar parameters as functions of axis ratio.

	$\frac{\lvert S_{HH}\rvert^2}{\lvert S_{VV}\rvert^2}$		$\lvert\nu\rvert$	
r	Actual	Estimated Eq. (5)	Actual	Estimated Eq. (9)
0.6	3.19	3.29	0.282	0.280
0.8	1.67	1.68	0.128	0.130
1.0	1.00	1.00	0.0	0.0
1.2	0.649	0.653	0.107	0.107
1.4	0.447	0.456	0.198	0.201

b. Circular depolarization ratio (CDR) Γ

For circularly polarized radar signals, the ratio of the power received with polarization orthogonal to the transmitted polarization to the power received with polarization identical to that transmitted defines the circular depolarization ratio (McCormick *et al.*, 1972). It has been shown (McCormick *et al.*, 1972; McCormick and Hendry, 1975) for time averaged power returns that this ratio may be expressed as

$$10^{\Gamma/10} = \frac{\int |\nu|^2 \sigma_c f(r) dr}{\int \sigma_c f(r) dr}, \tag{7}$$

where Γ is the circular depolarization ratio (CDR) in dB and $\sigma_c = \pi|S_{HH} + S_{VV}|^2$. In this instance of a distribution of uniformly sized drops, the integration is over the axis ratio distribution. In general, for any one drop, ν is a complex number defined (for right-hand circular polarization and zero canting angle) by

$$\nu = \frac{S_{VV} - S_{HH}}{S_{HH} + S_{VV}} = -|\nu| e^{i\phi}, \tag{8}$$

where $i = \sqrt{-1}$. At the wavelength of primary concern is this work (10.71 cm), $|\phi| < 0.04°$ and the exponential can be taken as unity. As the wavelength becomes shorter, however, the complex nature of ν becomes increasingly important.

From (7) the axis ratios observed in Miami were used to calculate Γ for monodisperse drop size distributions. Here Γ was computed using the observed axis ratio distributions, a Gaussian axis ratio distribution, and $\bar{r}$ alone (as described in the previous section). The computed values of Γ using the observed axis ratio distribution or the Gaussian form are essentially identical (Fig. 3). The Γ computed from $\bar{r}$ alone is considerably different. Since spherical particles do not contribute to the signal in the orthogonally polarized channel, Γ becomes very small when $\bar{r}$ is near unity. The spread of axis ratios when $\bar{r}$ is about one then becomes especially important since those r which depart significantly from unity produce most of the return in the orthogonal channel. It may be anticipated, therefore, that Γ should be sensitive to the spread (σ_r) in r as well as to $\bar{r}$.

This dependence of Γ on $\bar{r}$ and σ_r can be seen by noting that $|\nu|$ goes to zero as r goes to unity. Remembering the power law relation (5), it might be anticipated that $|\nu|$ may be related to $(1 - r)$ through a power law. Indeed, at 10.71 cm wavelength

$$|\nu| = 0.766(1 - r)^{1.10}, \quad 0.6 \leq r \leq 1, \tag{9a}$$

$$|\nu| = 0.462(r - 1)^{0.91}, \quad 1 < r \leq 1.4. \tag{9b}$$

Values of $|\nu|$ computed from (9) are compared to true values in Table 1. Although (9) is most accurate, $|\nu|$ can also be well represented by the linear relations

$$|\nu| = 0.697(1 - r), \quad 0.6 \leq r \leq 1, \tag{10a}$$

$$|\nu| = 0.496(r - 1), \quad 1 < r \leq 1.4. \tag{10b}$$

From (7) and (10a) it follows for oblate drops ($r \leq 1$)

$$10^{\Gamma/10} = \overline{|\nu|^2} \tag{11a}$$

$$= 0.486\overline{(1 - 2r + r^2)} \tag{11b}$$

$$= 0.486[(1 - \mathcal{R})^2 + \sigma_{\mathcal{R}}{}^2], \tag{11c}$$

where $\sigma_{\mathcal{R}}^2 = \overline{r^2} - \bar{r}^2$, the bar denotes a radar power average, and $\mathcal{R} \equiv \bar{r}$. $\sigma_{\mathcal{R}}^2$ will be referred to as the radar power weighted variance.

c. The polarization parameter ρ

Another polarization parameter that has been used in meteorological investigations is also derived from the circular polarization radar technique. This parameter is the time average magnitude of the cross-correlation function of the back-scattered signals in the main and orthogonal channels (McCormick *et al.*, 1972). At long radar wavelengths, this may be written as

$$\rho = \frac{\int |\nu| \sigma_c f(r) dr}{\left[\left(\int |\nu|^2 \sigma_c f(r) dr\right)\left(\int \sigma_c f(r) dr\right)\right]^{0.5}}. \tag{12}$$

For N drops of identical size and with the same axis ratio r, (12) becomes

$$\rho = \frac{N|\nu|\sigma_c}{[N^2|\nu|^2\sigma_c{}^2]^{0.5}} = 1. \tag{13}$$

For drops of identical size but with a distribution of axis ratios expression (12) becomes

$$\rho = \frac{\overline{|\nu|}}{(\overline{|\nu|^2})^{0.5}}, \tag{14a}$$

$$\rho \propto \frac{\overline{|1 - r|^{1.10}}}{(\overline{|1 - r|^{2.20}})^{0.5}}, \quad 0.6 \leq r \leq 1, \tag{14b}$$

where the bar denotes a radar power weighted (σ_c) average and (14b) was obtained from (14a) and (9a). ρ clearly depends on $\mathcal{R}$ (and, therefore, D, Fig. 4).

In addition to $\mathcal{R}$, ρ also depends on $\sigma_{\mathcal{R}}^2$. This becomes clear if it is again assumed for the moment that there are only oblate drops. Using (10a) and combining (14a) and (11a)

$$\rho = \frac{(1 - \mathcal{R})}{[(1 - \mathcal{R})^2 + \sigma_{\mathcal{R}}^2]^{0.5}}. \tag{15}$$

To summarize, for monodisperse drop size distributions with polydisperse axis ratio distributions, z_{DR} appears to depend only on a radar reflectivity weighted mean axis ratio. On the other hand CDR and ρ de-

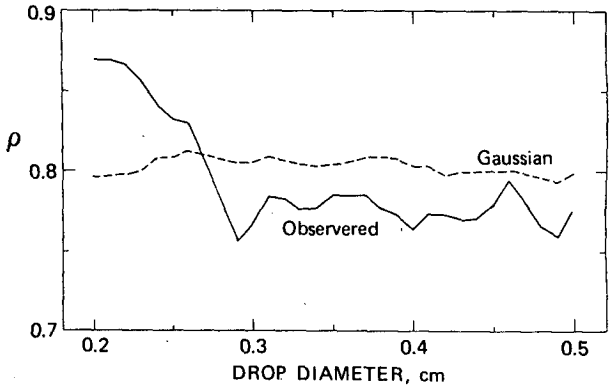

FIG. 4. The circular polarization variable ρ is plotted as a function of drop diameter for the Miami data. The solid line was computed using the observed axis ratio distribution at each drop size. The dashed line was computed for a Gaussian axis distribution with the average and standard deviation equal to those observed at each drop size.

pend on both a radar power weighted (σ_c) mean value of the axis ratio and on a radar power weighted variance of the drop axis ratio distribution. In principle, it should be possible to use Z_{DR} to obtain an estimate of the radar reflectivity weighted average axis ratio, while using a combination of CDR and ρ to provide an estimate of $\sigma^2_{\mathcal{R}}$.

In this section, monodisperse drop size distributions were used to investigate the sensitivity of Z_{DR}, Γ, and ρ to some properties of axis ratio distributions. In the real atmosphere, however, the radar polarization parameters are determined not only by the distribution of r corresponding to each drop size, but they are also strongly affected by the drop size distributions which are generally polydisperse. In the next section, estimators of radar power weighted $\mathcal{R}$ and $\sigma^2_{\mathcal{R}}$ will be developed that apply to both monodisperse and polydisperse drop size distributions.

4. Theoretically predicted polarization properties for polydisperse drop size distributions

For each polarization variable, the theoretical results from the previous section have been extended. When polydisperse drop size distributions are considered, however, matters become more complicated. To obtain results of greater generality, calculations were performed for a wide variety of drop size distributions and axis ratio distributions. In the remainder of the paper these computations will be referred to as the model calculations.

For each drop size it may be expected that some fraction of all the drops may be oscillating while the remainder will not. In the model calculations the fraction of drops at equilibrium and those oscillating was varied from 0 to 1. In general, therefore, it will be assumed that the axis ratio distribution will consist of a Dirac-delta distribution at the equilibrium axis ratio for the quiescent drops plus another axis ratio distribution for the oscillating drops component. This latter distribution was assumed to be Gaussian-shaped around a mean, $\bar{r}$. At each drop size the smallest $\bar{r}$ was assumed to be that at equilibrium, r_E. In successive calculations $\bar{r}$ was then incremented to a maximum value of $r_E + 0.15$. Although the mean axis ratio was never allowed to exceed unity, both oblate and prolate shapes were permitted. Values of the variance of the axis ratio distributions were specified by (2) with extrapolation to 0.1 cm at the lower end and 0.6 cm at the upper end.

The minimum drop size was varied from 0.01 cm to the maximum diameter which ranged from 0.12 to 0.6 cm. Initially the drop size distributions were assumed to be exponential, $N(D)dD = N_0 \exp[-\Lambda D]dD$ where $N(D)dD$ is the concentration of drops of size D to $D + dD$, Λ is the slope, and N_0 is a constant specified, in these calculations, by a fixed reflectivity factor. The slope was varied from 0 to 49 cm^{-1}. This range of conditions encompass monodisperse, and rectangular [uniform] distributions. Subsequent calculations were based on gamma distributions [$N(D)dD = N_0 D^2 \exp(-\Lambda D)dD$] and Gaussian-like distributions [$N(D)dD = N_0 D^{-1} \exp(-\Lambda^2 D^2)dD$].

The results of the calculations over all of the conditions described above produce expressions involving a number of constants. These have all been evaluated using a least square errors approach.

a. Z_{DR}

1) THEORETICAL EXTENSION TO POLYDISPERSE DROP SIZE DISTRIBUTIONS

When size distributions of drops are considered (4), (7), and (12) become more complicated. If $N(D)dD$ is the concentration of drops of size D to $D + dD$, (4) becomes

$$10^{-Z_{DR}/10} = \frac{\int N(D) \int |S_{VV}|^2 f(r) dr dD}{\int N(D) \int |S_{HH}|^2 f(r) dr dD}, \quad (16)$$

where $f(r)$ is the axis ratio distribution for drop size D normalized so that $\int f(r)dr = 1$. The integrals extend over all drop sizes and shapes. This equation can be rewritten as

$$10^{-Z_{DR}/10} = \frac{\int N(D) \int |S_{HH}|^2 r^{7/3} f(r) dr dD}{\int N(D) \int |S_{HH}|^2 f(r) dr dD} \quad (17a)$$

$$= \frac{\int N(D) \overline{r_D^{7/3}} \int |S_{HH}|^2 f(r) dr dD}{\int N(D) \int |S_{HH}|^2 f(r) dr dD}, \quad (17b)$$

where

$$\overline{r_D^{7/3}} = \frac{\int |S_{HH}|^2 r^{7/3} f(r) dr}{\int |S_{HH}|^2 f(r) dr}$$

is only a function of D. For each drop size, the integral over the axis ratio distribution which appears in the numerator and denominator of (17b) is the total contribution of all drops of one size D but different shapes to the horizontally polarized back-scatter return. Denoting the result of this integration by $|S_{HH}|_D^2$ (17b) can be rewritten as

$$10^{-Z_{DR}/10} = \frac{\int N(D)\overline{r_D^{7/3}}|S_{HH}|_D^2 dD}{\int N(D)|S_{HH}|_D^2 dD}, \quad (18a)$$

$$\equiv \overline{\mathcal{R}^{7/3}}, \quad (18b)$$

where $\mathcal{R}$ denotes a radar reflectivity weighting and the bar over denotes the averaging is over a drop size distribution.

A reflectivity weighted average $\bar{\mathcal{R}}$ is defined by

$$\bar{\mathcal{R}} \equiv \frac{\int N(D)\overline{r_D}|S_{HH}|_D^2 dD}{\int N(D)|S_{HH}|_D^2 dD}. \quad (19)$$

Since the integrals in (18) and (19) are over the same drop size distribution and axis ratio distributions, $\bar{\mathcal{R}}$ and $\overline{\mathcal{R}^{7/3}}$ must be related. An estimator of $\bar{\mathcal{R}}$ might be

$$\epsilon(\bar{\mathcal{R}}) = (10^{-Z_{DR}/10})^{3/7}. \quad (20)$$

The quality of the estimator will depend upon the closeness of $\bar{\mathcal{R}}^{7/3}$ to $\overline{\mathcal{R}^{7/3}}$. More specifically,

$$\frac{\epsilon(\bar{\mathcal{R}})}{\bar{\mathcal{R}}} = \frac{(\overline{\mathcal{R}^{7/3}})^{3/7}}{(\bar{\mathcal{R}}^{7/3})^{3/7}} \quad (21a)$$

$$\sim \left(\frac{\overline{\mathcal{R}^2}}{\bar{\mathcal{R}}^2}\right)^{0.5} \quad (21b)$$

$$\sim \left(1 + \frac{\sigma_{\mathcal{R}}^2}{\bar{\mathcal{R}}^2}\right)^{0.5}. \quad (21c)$$

The greater $\sigma_{\mathcal{R}}^2/\bar{\mathcal{R}}^2$, the greater is the difference between $\epsilon(\bar{\mathcal{R}})$ and $\bar{\mathcal{R}}$. An upper limit to $\sigma_{\mathcal{R}}^2/\bar{\mathcal{R}}^2$ might be approximated by considering a drop distribution consisting of two widely separated diameters (say at 0.1 cm and 0.6 cm, for example) but both contributing equally to the total reflectivity factor. If in addition it is assumed that D and r are related by (1b), then $\overline{\mathcal{R}^2} = 0.684$ and $\bar{\mathcal{R}}^2 = 0.661$ and $\sigma_{\mathcal{R}}^2/\bar{\mathcal{R}}^2 \approx 0.04$. From (21c) $\epsilon(\bar{\mathcal{R}})/\bar{\mathcal{R}} \sim 1.02$. Since this example is rather extreme, in practice, $\epsilon(\bar{\mathcal{R}})$ may be expected to usually provide reasonably accurate estimates of $\bar{\mathcal{R}}$. It is, therefore, permissible to write

$$\bar{\mathcal{R}} = (10^{-Z_{DR}/10})^{0.43}. \quad (22)$$

This relation should be useful for many meteorological conditions.

2) Model calculations

To substantiate (22), $\bar{\mathcal{R}}$ and $\epsilon(\bar{\mathcal{R}})$ were determined from the model calculations. The results showed that

$$\bar{\mathcal{R}} = 1.01(10^{-Z_{DR}/10})^{0.42}, \quad (23)$$

with a correlation coefficient of −0.99. In these computations the associated standard error of the estimate is 0.0093. Since (22) and (23) are quite similar, it seems safe to conclude that Z_{DR} does seem to measure the reflectivity weighted average axis ratio $\bar{\mathcal{R}}$. Although this is not surprising, it is important to establish the explicit relationship tying Z_{DR} to shape.

To illustrate the application of (22) and (23) to specific examples of single drop size distributions, $\bar{\mathcal{R}}$ was calculated and then estimated using (22) and (23) for an exponential, gamma, Gaussian-like, rectangular, monodisperse, and bimodal drop size distribution. The results are shown in Table 2. The largest difference between the calculated $\bar{\mathcal{R}}$ and that estimated from (23) occurs for the bimodal distribution in which 0.1 cm and 0.6 cm drops contribute equally to the radar return power. In that sense, this distribution represents a worst case.

b. Circular depolarization ratio (CDR), Γ and ρ

1) Theoretical extension to polydisperse drop size distributions

As (11) indicates, Γ is strongly affected by both the mean and variance of the axis ratio distribution. By itself, therefore, Γ is not likely to be as good an estimator of $\bar{\mathcal{R}}$ as Z_{DR}. Since ρ and Γ are functions of both $\bar{\mathcal{R}}$ and $\sigma_{\mathcal{R}}^2$, however, it might be possible to extract estimators of $\sigma_{\mathcal{R}}^2$ and $\bar{\mathcal{R}}$ from combinations of ρ and Γ.

For a polydisperse drop size distribution (12) becomes

$$\rho = \frac{\int N(D) \int |\nu|\sigma_c f(r) dr dD}{\left[\left(\int N(D) \int |\nu|^2 \sigma_c f(r) dr dD\right) \times \left(\int N(D) \int \sigma_c f(r) dr dD\right)\right]^{0.5}} \quad (24a)$$

$$= \frac{\int N(D)\overline{|\nu|}_D \sigma_{cD} dD}{\left[\left(\int N(D)\overline{|\nu|^2}_D \sigma_{cD} dD\right)\left(\int N(D)\sigma_{cD} dD\right)\right]^{0.5}} \quad (24b)$$

TABLE 2. Calculated and estimated values of $\bar{\mathcal{R}}$.

	D_{min} (cm)	D_{max} (cm)	Λ (cm^{-1})	N_0 (cm^{-4})	$\bar{\mathcal{R}}_{calc}$	$\bar{\mathcal{R}}_{est}$ Eq. (23)	$\bar{\mathcal{R}}_{est}$ Eq. (22)
Exponential	0.01	0.6	20	0.1855	0.912	0.914	0.903
Gamma	0.01	0.6	10	0.2401	0.658	0.664	0.660
Gaussian-like	0.01	0.6	10	0.052	0.929	0.937	0.927
Rectangular	0.01	0.6	0	7.50×10^{-7}	0.707	0.716	0.744
Monodisperse	0.30	0.30	—	0.0185	0.844	0.856	0.844
Bimodal	0.10	0.60	—	Equal Powers	0.894	0.851	0.842

$$= \frac{\overline{\overline{|v|}}}{(\overline{\overline{|v|^2}})^{0.5}}, \tag{24c}$$

where

$$\overline{|v|}_D = \frac{\int |v|\sigma_c f(r)dr}{\int \sigma_c f(r)dr}, \quad \sigma_{cD} = \int \sigma_c f(r)dr$$

and the double bar indicates a power weighted (σ_{cD}) average over the drop size distribution. From the definition of variance, (24c) yields

$$1 - \rho^2 = \frac{\sigma^2_{|v|}}{\overline{\overline{|v|^2}}}, \tag{25}$$

where $\sigma^2_{|v|} = \overline{\overline{|v|^2}} - \overline{\overline{|v|}}^2$. The quantity $1 - \rho^2$ is, therefore, a measure of the relative dispersion of $|v|$ which is intimately related to the spread in the drop shapes. Now

$$10^{\Gamma/10} = \frac{\int N(D) \int |v|^2 \sigma_c f(r)drdD}{\int N(D) \int \sigma_c f(r)drdD} \tag{26a}$$

$$= \frac{\int N(D)\overline{|v|^2}_D \sigma_{cD} dD}{\int N(D)\sigma_{cD} dD} \tag{26b}$$

$$= \overline{\overline{|v|^2}}, \tag{26c}$$

where

$$\overline{|v|^2}_D = \frac{\int |v|^2 \sigma_c f(r)dr}{\int \sigma_c f(r)dr}.$$

Expression (25) becomes

$$\sigma^2_{|v|} = (1 - \rho^2)10^{\Gamma/10}. \tag{27}$$

Therefore Γ and ρ give a measure of the variance of $|v|$.

This variance, however, is related to $\sigma^2_{\mathcal{R}}$. If we assume that all drops are oblates and if we use (10a), then

$$\overline{\overline{|v|}} = 0.697(1 - \bar{\mathcal{R}}) \tag{28a}$$

or

$$\overline{\overline{|v|^2}} = 0.486(1 - 2\bar{\mathcal{R}} + \overline{\mathcal{R}^2}). \tag{28b}$$

In this case

$$\sigma^2_{|v|} = 0.486\sigma^2_{\mathcal{R}}, \tag{29}$$

where $\sigma^2_{\mathcal{R}} = \overline{\mathcal{R}^2} - \bar{\mathcal{R}}^2$. Combining (27) and (29),

$$\sigma^2_{\mathcal{R}} = 2.06(1 - \rho^2)10^{\Gamma/10}. \tag{30}$$

With $\sigma^2_{\mathcal{R}}$ it is then possible to estimate $\bar{\mathcal{R}}$ from measurements of Γ. From the definition of variance and (30) we can also write

$$\bar{\mathcal{R}} = 1 - (2.06\ 10^{\Gamma/10} - \sigma^2_{\mathcal{R}})^{0.5}, \tag{31}$$

where $\sigma^2_{\mathcal{R}}$ is calculated from (30).

2) MODEL CALCULATIONS

The $\bar{\mathcal{R}}$ and $\sigma^2_{\mathcal{R}}$ were determined from the model calculations described earlier. These calculations suggest that

$$\sigma^2_{\mathcal{R}} = 2.56[(1 - \rho^2)10^{\Gamma/10}]^{1.01}, \tag{32}$$

$$\bar{\mathcal{R}} = 1 - 0.96(2.28\ 10^{\Gamma/10} - \sigma^2_{\mathcal{R}})^{0.50}, \tag{33}$$

where $\sigma^2_{\mathcal{R}}$ is obtained from (32). The correlation coefficients for (32) and (33) are both 0.99. In these computations the corresponding standard errors of the estimates are 0.0016 and 0.0099, respectively.

Both (32) and (33) are close to the expected forms (30) and (31). It should be remembered, however, that in the derivation of (30) it was assumed that $r \leqslant 1$. In the unlikely event that all drops are prolates ($r \geqslant 1$), (10b) implies that the coefficient in (30) would become 4.06 while the remainder of the expression would be unaltered. It might be expected, that in a drop ensemble which is a mixture of oblate and prolate drops, the coefficient for (30) would tend to increase as the proportion of the radar return due to prolate drops increases. Since some times both prolate and oblate drops coexisted in the computations leading to (32), the greater coefficient in (32) compared to that in (30) may be explained by this effect. It could, of course, also be explained by the fact that the relation between $|v|$ and $(1 - r)$ is not precisely linear [i.e., expression (9a)]. In situations when few

if any prolate drops are present, the coefficient in (32) may approach that in (30). Insofar, as the model calculations encompass a wide range of meteorologically plausible conditions, however, (32) and (33) probably provide reasonable estimates of $\sigma^2_{\mathcal{R}}$ and $\bar{\mathcal{R}}$ for many rain situations.

Although (33) appears to be just as good an estimator of $\bar{\mathcal{R}}$ as (23), it involves two measurables. This estimator, therefore, is more indirect and, in practice, may be subject to more uncertainty than $\mathcal{R}$ derived from (23). Although Γ and Z_{DR} are distinctly different (23) and (33) show that they are related and, in principle, could be combined to yield estimates of $\sigma^2_{\mathcal{R}}$.

To illustrate the use of (32) and (33), sample calculations for individual drop size distributions are shown in Table 3.

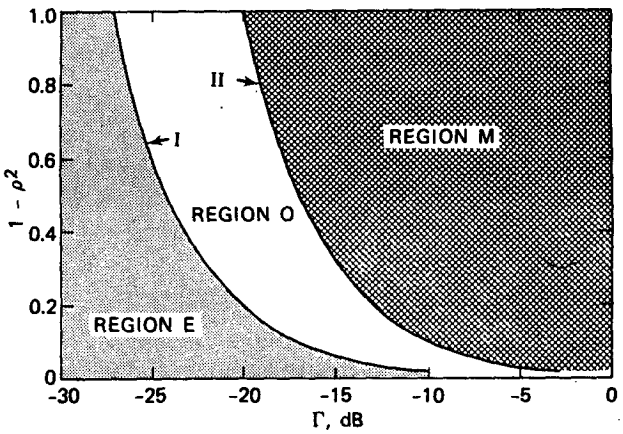

FIG. 5. Plot of $1 - \rho^2$ versus Γ, the circular depolarization ratio. Lines I and II correspond to constant values of the variance of the axis ratio distribution. As explained in the text, observations in rain are not expected to fall in the hatched region M. Size distributions of quiescent, equilibrium shaped drops are expected to lie mostly to the left of I in the shaded region E. The zone between I and II (region O) is expected to contain size distributions of oscillating drops for which there is a distribution of axis ratios for each drop diameter.

5. Discussion

This work has concentrated on an interpretation of some of the measurables provided by circular and linear polarization radar techniques and the use of these measurables to estimate the radar power weighted mean $\bar{\mathcal{R}}$ and standard deviation $\sigma^2_{\mathcal{R}}$ of the raindrop axis ratio distribution. As a result of power law relations between the axis ratio and combinations of elements in the back-scatter matrix, estimators of $\bar{\mathcal{R}}$ and $\sigma^2_{\mathcal{R}}$ were developed which appear to be applicable to a wide variety of drop size distributions. The estimators (32) and (33) were evolved for a radar wavelength of 10.71 cm. Subsequent computations, however, indicate that the forms of (32) and (33) are valid down to at least a wavelength of 3.21 cm although some of the coefficients are altered. At even shorter wavelengths, raindrops are predominately in the Mie scattering regime, and the applicability of results of this study is not known.

The potential uses of the information provided by estimates of $\bar{\mathcal{R}}$ and $\sigma^2_{\mathcal{R}}$ are yet to be fully explored. As one example, measurements of ρ and Γ (CDR) could be used to help evaluate the extent to which raindrops above the surface layer oscillate. In all the model calculations in this study, for example, the largest value of $\sigma^2_{\mathcal{R}}$ found for quiescent drops having equilibrium shapes was 0.005. From (32), this value defines line I in Fig. 5. Insofar, as this value of $\sigma^2_{\mathcal{R}}$ represents a reasonable upper limit, values of $1 - \rho^2$ and Γ produced by distributions of quiescent, equilibrium shaped drops should lie in the shaded region E. Similarly, line II is defined by $\sigma^2_{\mathcal{R}} = 0.026$, the largest value found in any of the model calculations. In the absence of ice, any measurements lying between lines I and II (region O) could then be interpreted as evidence for raindrop oscillation. Points to the right of line II (region M) cannot be produced by rain alone and measurements in that region would presumably be an indication of non-spherical ice. These interpretations assume, of course, for any particular set of measurements that the observed drop size distributions are similar to those used in the model calculations.

Unfortunately, there are very few published data sets presenting simultaneous measurements of ρ and Γ at long wavelengths. One such study (16 August 1978), however, is discussed by Humphries and Barge (1979). In that investigation, values of $\rho = 0.4$ and $\Gamma = -12$ dB were measured near the center of the bright band. This point clearly lies in region M (Fig. 5). Six hundred meters lower, probably a sufficient

TABLE 3. Sample calculations for individual drop size distributions.

	D_{min} (cm)	D_{max} (cm)	Λ (cm^{-1})	N_0 (cm^{-4})	$\sigma^2_{\mathcal{R}}$ calculated	$\sigma^2_{\mathcal{R}}$ estimated Eq. (31)	$\bar{\mathcal{R}}$ calculated	$\bar{\mathcal{R}}_{est}$ Eq. (32)
Exponential	0.01	0.6	20	0.1855	4.38×10^{-3}	4.64×10^{-3}	0.912	0.915
Gamma	0.01	0.6	10	0.2401	0.63×10^{-6}	0.0	0.658	0.656
Gaussion-like	0.01	0.6	10	5.16×10^{-3}	1.17×10^{-3}	1.08×10^{-3}	0.929	0.936
Rectangular	0.01	0.6	0	7.05×10^{-7}	1.79×10^{-3}	2.48×10^{-3}	0.707	0.708
Monodisperse	0.30	0.30	—	0.0185	5.96×10^{-7}	0.0	0.844	0.857
Bimodal	0.10	0.60	—	equal Power	2.88×10^{-2}	3.40×10^{-2}	0.894	0.858

distance for snow and low density graupel to melt in summer, $\rho = 0.75$ and $\Gamma = -22$ dB. This point lies squarely in the region O in Fig. 5. If melting were indeed complete, this could well be interpreted as evidence for the presence of oscillating raindrops. One must be cautious, however, about accepting such an interpretation based on one or two measurements. For example, if the drop size distribution were bimodal with significant radar power contributions coming from both drop sizes, then even if the drops were quiescent and equilibrium shaped, $\sigma^2_{\bar{R}}$ could exceed the threshold of 0.005 which defines the boundary between regions E and O.

Using much more extensive data typical values of ρ and Γ measured at a wavelength of 10.4 cm in stratiform and convective rain are reported by Hendry *et al.* (1976). These are plotted in Fig. 6. It appears that in many stratiform rains the raindrops may be nearly equiescent and equilibrium shaped. In contrast, in many convective rains, it appears that often some of the raindrops are oscillating. These results agree with conclusions reached after considering the effect of raindrop collisions on raindrop oscillation in stratiform (light) rains and convective (heavy) rains (Beard *et al.*, 1983).

In another case (30 August 1979) aircraft observed snow descending to the 0°C level at around 2.1 km, MSL. The height profile of ρ and Γ is plotted in Fig. 6. Above the 0°C level, snow produces the radar signals. At 300 m below the 0°C level, the measurements shift into the region where the snow is presumably wet and melting. By 900 m below the 0°C level ρ and Γ have changed substantially. At that height, $\rho = 0.63$ and $\Gamma = -21$ dB which might also be interpreted as evidence for the presence of oscillating raindrops. From (33) the particular value of $\bar{R}$ corresponding to these latter values of ρ and Γ is 0.923 indicating the presence of drops with diameters larger than 0.17 cm.

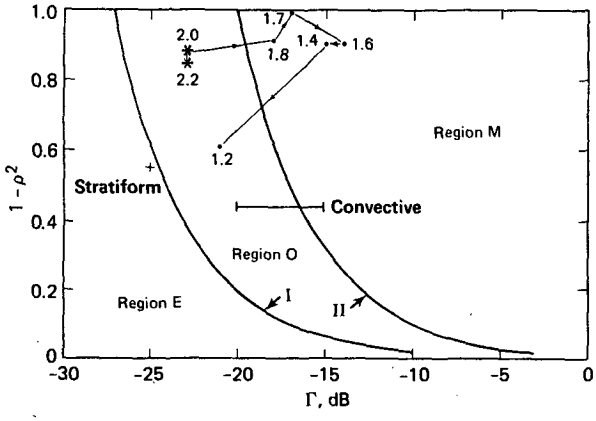

FIG. 6. As in Fig. 5 except that the height profile through a radar bright band (from Humphries and Barge, 1979) is plotted. The numbers denote km MSL. The 0°C level was at 2.1 km. The asterisks denote snow as observed by aircraft. The cross and horizontal bar indicate typical locations of measurements made at 10.4 cm wavelength in stratiform rain and convective rain (Hendry *et al.*, 1976), respectively.

Even though many of the equations developed in this paper are not strictly applicable to conditions at peak intensity of the bright band, it is interesting to note that if the precipitation were horizontally oriented, the small value of ρ (large values of $1 - \rho^2$) coupled with the larger value of Γ suggest a large variance of axis ratios, i.e., that there is an unusually large range of particle shapes. This is to be expected in a region containing wet and melting snow along with small raindrops.

Although estimates of $\bar{R}$ and $\sigma^2_{\bar{R}}$ are useful, as the example above suggests, the analysis of these polarization quantities can be extended. In rain, it should generally be safe to assume that smaller and smaller axis ratios are associated with larger and larger drops. It then follows that a small variance of axis ratios is suggestive of a narrower distribution of drop sizes while a large variance is suggestive of a wider range of drop sizes. This suggests that a method may exist for translating estimates of $\bar{R}$ and $\sigma^2_{\bar{R}}$ into estimates of $\bar{D}$ and σ^2_D, the power weighted mean diameter and variance of the drop size distribution. In the companion paper (Jameson, 1983b), a method for this transformation which does not invoke detailed assumptions about the exact form of the drop size distribution or the exact relationship between drop size and shape is presented. This transformation also leads to the development of estimators for rainwater content and rainfall rate in still air.

Acknowledgments. The author is greatly indebted to Dr. Charles Warner at the University of Virginia for his very gracious generosity in providing the program used to calculate the raindrop scattering functions used in this work. The most recent version of the computational techniques is described by Dr. Warner in a report "Calculated Scattering Characteristics of Hailstones at Weather Radar Wavelengths," to the Alberta Research Council. Dr. David B. Johnson of the Illinois State Water Survey provided invaluable comments which greatly clarified this manuscript. This work was supported by the National Science Foundation under Grants NSF ATM79-18365 and NSF ATM81-08455.

REFERENCES

Barge, B. L., 1974: Polarization measurements of precipitation backscatter in Alberta. *J. Rech. Atmos.*, **8**, 163–173.

Beard, K. V., and A. R. Jameson, 1983: Raindrop canting. *J. Atmos. Sci.*, **40**, 448–454.

——, D. B. Johnson and A. R. Jameson, 1983: Collisional forcing of raindrop oscillation. *J. Atmos. Sci.*, **40**, 455–462.

Blanchard, D. C., 1950: The behavior of water drops at terminal velocity in air. *Trans. Amer. Geophys. Union*, **31**, 836–842.

——, 1962: Comments on the breakup of raindrops. *J. Atmos. Sci.*, **19**, 119–120.

Bresch, J. F., 1982: Raindrop axis ratios. M.S. thesis, Dept. Atmos. Sci., University of Illinois.

Brook, M., and D. J. Latham, 1968: Fluctuating radar echo: Modulation by vibrating drops. *J. Geophys. Res.*, **73,** 7137–7144.

Brussard, G., 1974: Rain-induced cross-polarization and raindrop canting. *Electron. Lett.*, **10,** 411–412.

Crispin, J. W., and K. M. Siegel, 1968: *Methods of Radar Cross Section Analysis,* Academic Press, 426 pp.

Deschamps, G. A., 1951: Geometrical representation of the polarization of a plane electromagnetic wave. *Proc. I.R.E.*, **39,** 540–544.

Goddard, J. W. F., S. M. Cherry and V. N. Bringi, 1982: Comparison of dual-polarization radar measurements of rain with ground-based distrometer measurements. *J. Appl. Meteor.*, **21,** 252–256.

Hall, M. P. M., S. M. Cherry, J. W. F. Goddard and G. R. Kennedy, 1980: Raindrop sizes and rainfall rate measured by dual-polarization radar. *Nature,* **285,** 195–198.

Hendry, A., and G. C. McCormick, 1974: Polarization properties of precipitation particles related to storm structure. *J. Rech. Atmos.*, **8,** 189–200.

——, —— and B. L. Barge, 1976: The degree of common orientation of hydrometeors observed by polarization diversity radars. *J. Appl. Meteor.*, **15,** 633–640.

Humphries, R. G., and B. L. Barge, 1979: Polarization and dual-wavelength radar observations of the bright band. *I.E.E.E. Trans. Geosci. Electron.*, **GE-17,** 190–195.

Jameson, A. R., 1983b: Microphysical interpretation of multi-parameter radar measurements in rain. Part II: Estimation of raindrop distribution parameters by combined dual-wavelength and polarization measurements. *J. Atmos. Sci.*, **40,** 1803–1813.

——, and K. V. Beard, 1982: Raindrop axial ratios. *J. Appl. Meteor.*, **21,** 257–259.

Jones, D. M. A., 1959: The shape of raindrops. *J. Meteor.*, **16,** 504–510.

Maher, B. O., P. J. Murphy and M. C. Sexton, 1977: A theoretical model of the effect of wind gusting on rain-induced cross-polarization. *Ann. Télécommun.*, **32,** 404–408.

McCormick, G. C., and A. Hendry, 1975: Principles for the determination of the polarization properties of precipitation. *Radio Sci.*, **10,** 421–434.

——, and ——, 1979: Techniques for the determination of the polarization properties of precipitation. *Radio Sci.*, **14,** 1027–1040.

——, —— and B. L. Barge, 1972: The anisotropy of precipitation media. *Nature,* **238,** 214–216.

Mueller, E. A., and A. L. Sims, 1966: Investigation of the quantitative determination of point and areal precipitation by radar echo measurements. Tech. Rep. ECOM-00032-F, U.S. Army Signal Corps, 88 pp. [NTIS AD645218].

Nelson, A. R., and N. R. Gokhale, 1972: Oscillation frequencies of freely suspended water drops. *J. Geophys. Res.*, **77,** 2724–2727.

Pruppacher, H. R., and K. V. Beard, 1970: A wind tunnel investigation of the internal circulation and shape of water drops falling at terminal velocity in air. *Quart. J. Roy. Meteor. Soc.*, **96,** 247–256.

——, and R. L. Pitter, 1971: A semi-empirical determination of the shape of cloud and rain drops. *J. Atmos. Sci.*, **28,** 86–94.

Seliga, T. A., and V. N. Bringi, 1976: Potential use of radar differential reflectivity measurements at orthogonal polarizations for measuring precipitation. *J. Appl. Meteor.*, **15,** 69–76.

Warner, C., and A. Hizal, 1976: Scattering and depolarization of microwaves by spheroidal raindrops. *Radio Sci.*, **11,** 921–930.